Failure analysis based on microvoid growth for sheet metal during uniaxial and biaxial tensile tests

Fethi Abbassi [a,*], Sebastien Mistou [b], Ali Zghal [a]

[a] URMSSDT, ESSTT, University of Tunis, 5 Avenue Taha Hussein, BP, 56, Bâb Manara 1008, Tunisia
[b] Université de Toulouse, INP/ENIT, M2SP-LGP, 47 Avenue d'Azereix, 65016 Tarbes, France

Keywords:
Tensile test
Fractography
Numerical modeling
Damage model
Necking
Microvoid growth

A B S T R A C T

The aim of the presented investigations is to perform an analysis of fracture and instability during simple and complex load testing by addressing the influence of ductile damage evolution in necking processes. In this context, an improved experimental methodology was developed and successfully used to evaluate localization of deformation during uniaxial and biaxial tensile tests. The biaxial tensile tests are carried out using cruciform specimen loaded using a biaxial testing machine. In this experimental investigation, Stereo-Image Correlation technique has is used to produce the heterogeneous deformations map within the specimen surface. Scanning electron microscope is used to evaluate the fracture mechanism and the micro-voids growth. A finite element model of uniaxial and biaxial tensile tests are developed, where a ductile damage model Gurson–Tvergaard–Needleman (GTN) is used to describe material deformation involving damage evolution. Comparison between the experimental and the simulation results show the accuracy of the finite element model to predict the instability phenomenon. The advanced measurement techniques contribute to understand better the ductile fracture mechanism.

1. Introduction

The finite elements method (FEM) is one of the most important approaches used to design mechanical parts, in large strain field. A successful simulation requires the availability of a reliable stress–strain curve [1]. Before necking, these curves can be obtained easily, but their identification becomes complex beyond the onset of necking [2]. In effect, when localized necking commences, the strain distribution at the minimum cross-section becomes highly non-uniform [3]. Moreover analysis and modeling of this phenomenon are important, because in most industrial cases the necking and strain localization are a crucial precursors to the final failure. They determine the maximal amount of thinning that the metal sheet can undergo in various areas. The localization behavior of a material is due to two reasons: (i) The material non-homogeneities (second phase particles, grain morphology of surface defects, etc.) [4–8], (ii) constitutive behavior (material strain hardening, softening and rate sensitivity, etc.) [9,10].

In this investigation, the Stereo-Image Correlation (SIC) method is used to evaluate the necking and localization of deformation in uniaxial tensile and biaxial tests. In this experimental part, a mild steel sheet material was investigated with a thickness of 4 mm. A digitalization of the useful zone (central zone) of cruciform specimen after the test allowed to analyze the necking phenomenon and the localization of deformation, which precedes the fracture. Important information about ductile damage evolution and accumulation mechanism can be gathered upon the examination of the fracture zone and the necking region using scanning electron microscope (SEM). These microstructure analysis results represent the key of the ductile damage model used in numerical simulation. Different cruciform geometries have been investigated numerically using a finite element method. This way led to a number of design guidelines to avoid unwanted failure modes for the miniaturized setup. In the modeling of uniaxial tensile and biaxial tests, we use the model of Gurson Tvergaard Needleman (GTN) to describe the damage evolution during load application. The results of finite element simulations are compared with experimental results, and a good correlation is observed.

2. Experimental setup and methods

2.1. Full-field Stereo Image Correlation measurements

The images correlation allows the measurement of displacement fields of a planar surface: a single camera acquires a sequence of images of a planar object under loaded conditions. But single-camera, 2-D Digital Image Correlation (DIC) systems are limited to planar specimens that experience little or no out-of-plane motion. These limitations can be overcome by the use of two or more

* Corresponding author. Tel.: +216 96 167 265; fax: +216 71 391 166.
E-mail address: fethi.abbassi@ipeib.rnu.tn (F. Abbassi).

cameras observing the surface from different directions. The combination of these cameras during experimental measurements is called stereo-vision or SIC. This method is widely applied in measuring full-field displacements during metal forming process in recent years especially for out of plan displacements. The extensive use of this advanced measurement technique can be explained by the inability of traditional measuring approaches (strain gauge and extensometer) to collect enough information such as the localization of deformations. One of the principal advantages of the full-field measurements is that the selection of the measurement points is flexible since it can be carried out after the experiment [11]. The principal devices of SIC, 3D image correlation software, light source and two CCD cameras to acquire digital images with a 1280 by 1024 pixel. These images are then analyzed by the Aramis software developed by GOM. This gives a measure of the displacements and strain fields on the surface of an object within a good precision. Aramis software is able to match corresponding points of an image by grey level analysis, if the surface of the specimen is covered with a black and white mapping, which forms a random grey-level of grey. A gray level coded on 8 or 12 bits corresponds to each pixel of the CCD sensor. A succession of several pixels lying on the same line forms a grey level sequence. The fundamental principle lies in the fact that the distribution does not vary during the deformation of the body. It is therefore sufficient to follow this distribution of grey levels in their motion to obtain the displacements of the corresponding point. Fig. 1 shows a stereo-vision system with two CCD cameras, different coordinate systems and epipolar lines constrain search region within images to locations along a line. Corresponding image points for object point P (x,y,z) in camera 1 and camera 2 are P_1 and P_2 respectively. All these coordinate systems are interconnected by several transformation matrices, which require an important step during experiment setup known calibration. The later consists of assessing the baseline transformation (determination of matrix related the two cameras coordinates system) and in calculating of intrinsic parameters of the cameras [11]. Generally two approaches are used to calibrate cameras in stereo correlation setup. The first approach calibrates each camera separately and the second calibrates the two cameras together. The latter is known as a stereo-rig [12].

2.2. Uniaxial tensile tests setup

A tensile test is one of the most important engineering procedures for deriving the mechanical behavior of materials. In this work, the tension test was conducted under displacement control in an Instron testing machine, which runs at a rate of 3.10^{-4} mm/s, at room temperature. The load–displacement response of the material are measured in a tensile test on the specially designed specimen [13] shown in Fig. 2a. Two CCD cameras are positioned in a non-symmetrical configuration: first one directly in front of the specimen and the second one at about 32° from the normal. This allows performing 3D full-field displacement measurement. The images recorded during the test correlated with Aramis software, Fig. 2b shows an example of the displacements map with 3D coordinates.

2.3. Biaxial tensile tests

One of the most challenging aspects of a biaxial testing system is test specimen design, which restricts application for the cruciform biaxial tensile test. Several specimens of the cruciform type have been investigated quite extensively. However there is no standard geometry exists, therefore it is difficult to compare the test results obtained by different investigators [14]. After many iterations, the desired final geometry of cruciform specimen is show in Fig. 3. We prepare the cruciform specimens using laser cutting of the external contour and turning process with CNC machine to reduce the thickness up to 1 mm in the gauge area. These specimens are oriented 0° and 45° with respect to the rolling direction of sheet in order to take account of the anisotropy of the sheet. The biaxial tensile tests are performed using INSTRON 8800 biaxial machine available in the LGP laboratory (Fig. 4). Before the start of the biaxial test, a variable grey level is developed in the surface of

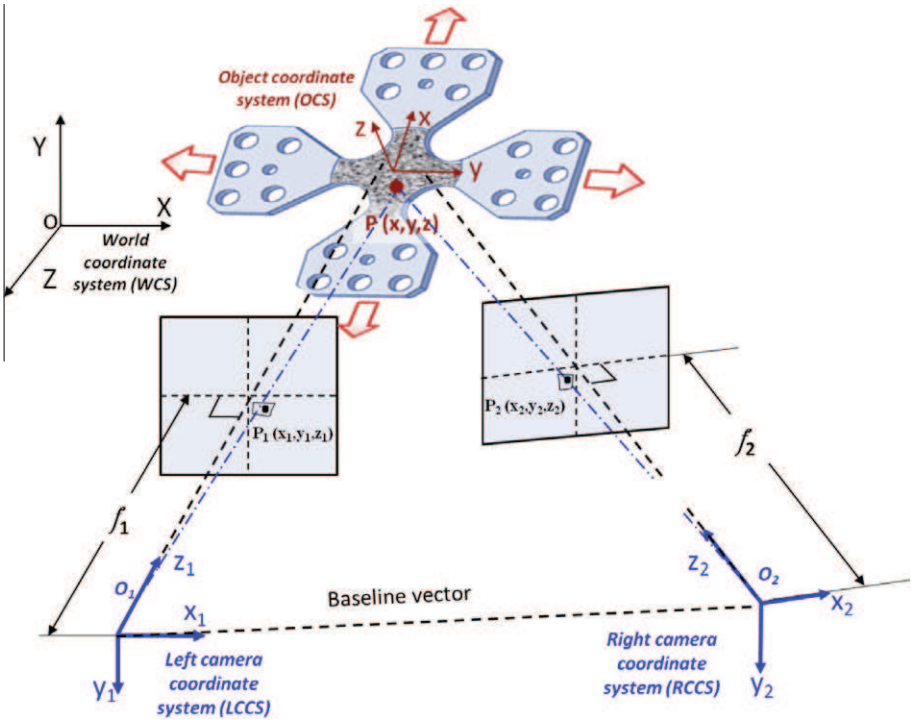

Fig. 1. Schematic of two camera stereo-vision system.

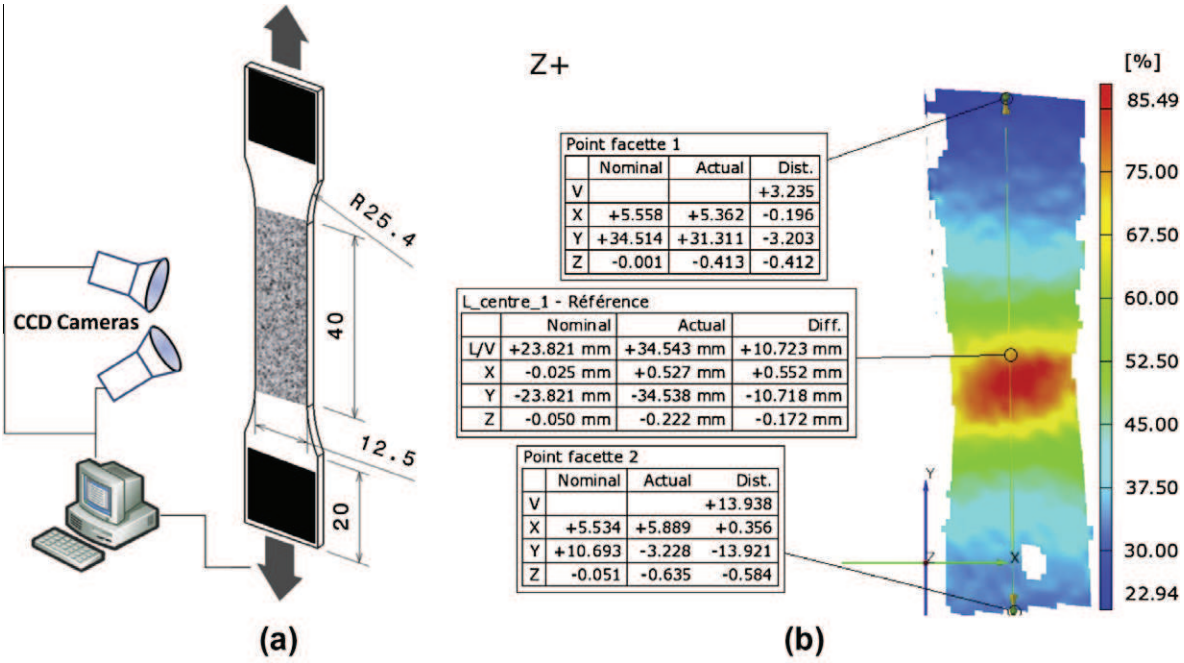

Fig. 2. (a) Uniaxial tensile specimens designed and (b) typical results extracted using SIC, deformation and 3D coordinates.

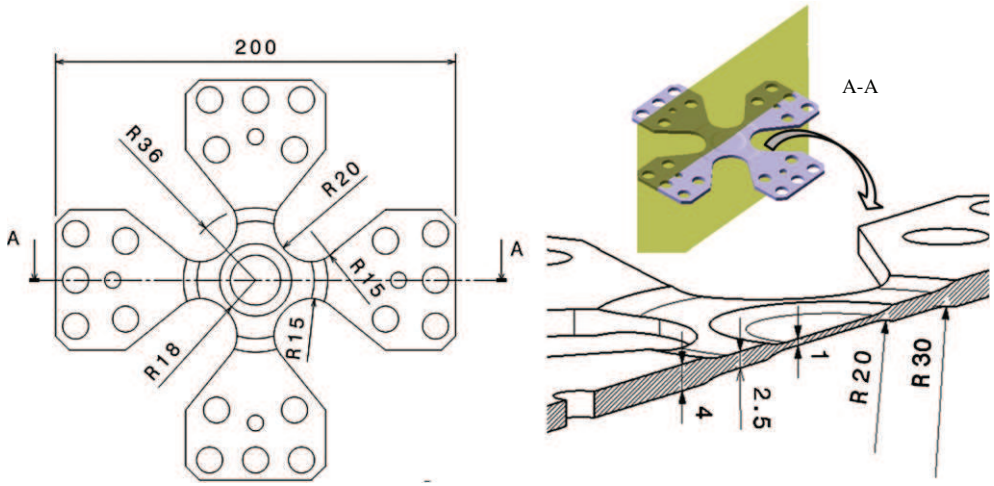

Fig. 3. Designed cruciform tensile specimen with dimensions (mm).

the sample in order to measure the displacement field in selected specimen gauge areas with Stereo Image Correlation method.

Fig. 4 shows the setup of biaxial tensile test, two cameras are installed in front of the specimen. A cross-shaped specimen is loaded in the biaxial testing machine in an equi-biaxial manner. Fig. 5 shows typical results of equi-biaxial test, the displacements field obtained by SIC in the surface of specimen oriented 45° respecting the rolling direction. In this displacement maps, we observe that the results in the two directions are similar which is coherent with the reality, because the two axis of cruciform specimen oriented 45° with the rolling direction.

3. Failure analysis (fractography)

In metal forming investigation, fractography is used to analyze the nature of failure and the formability of material [15], fracture surfaces of tensile sample has been obtained using scanning electron microscope.

- Fig. 6 shows the fracture revealing a shear mechanism leading to failure. The dimples in vicinity of the shear zone are elongated in the direction of shear, is as indicative of ductile fracture mode.
- A ductile fracture mechanism is dominant where a large number of dimples can be observed in Fig. 7. The rupture surface itself shows large regions of dimples, the larger ones including second phase particles [16]. We observe the average void sizes are bigger, that refers to the ductile fracture [17].
- The initiation of failure is governed by void nucleation and growth. This is evident from Fig. 8, that the coalescence of the cavities, the growth of microvoids for an increasing plastic deformation progressively reduces the material capability to support the mechanical loads up to complete failure [18].

This implies that modeling of damage evolution, crack initiation, and crack extension should be based on porous metal plasticity. The Gurson modified model called GTN [19] model is able to describe the different stage of this ductile crack phenomena.

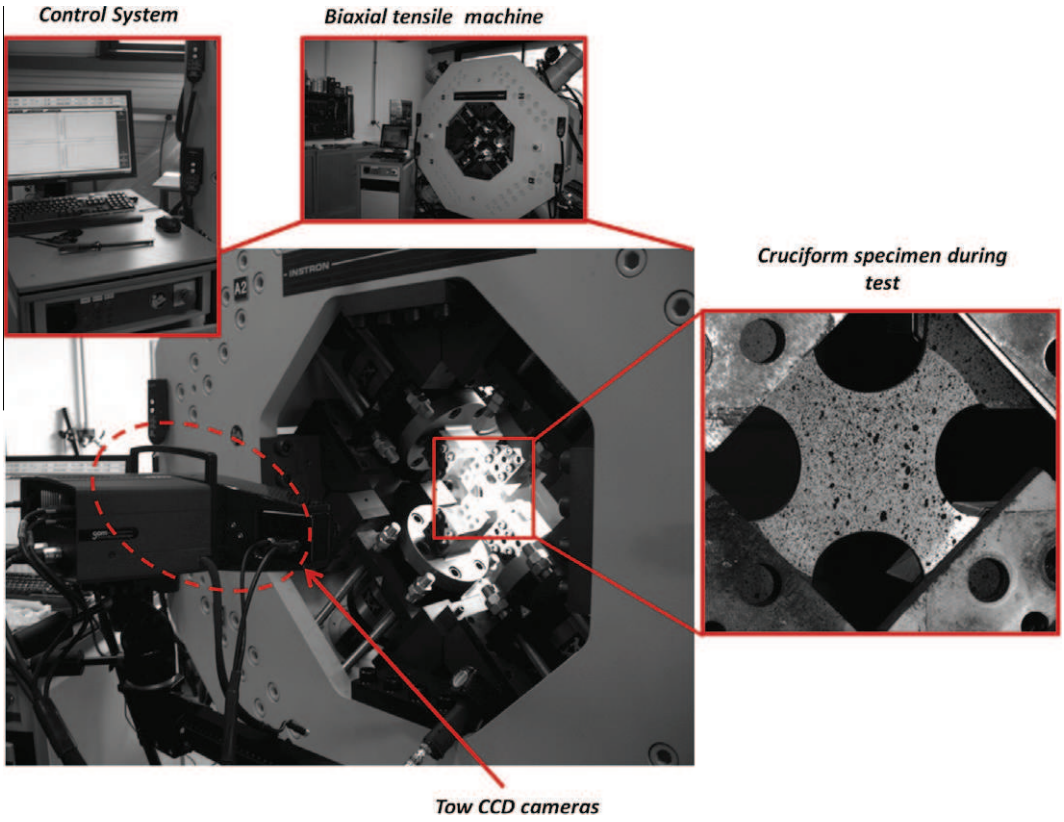

Fig. 4. Experimental setup for biaxial tensile test.

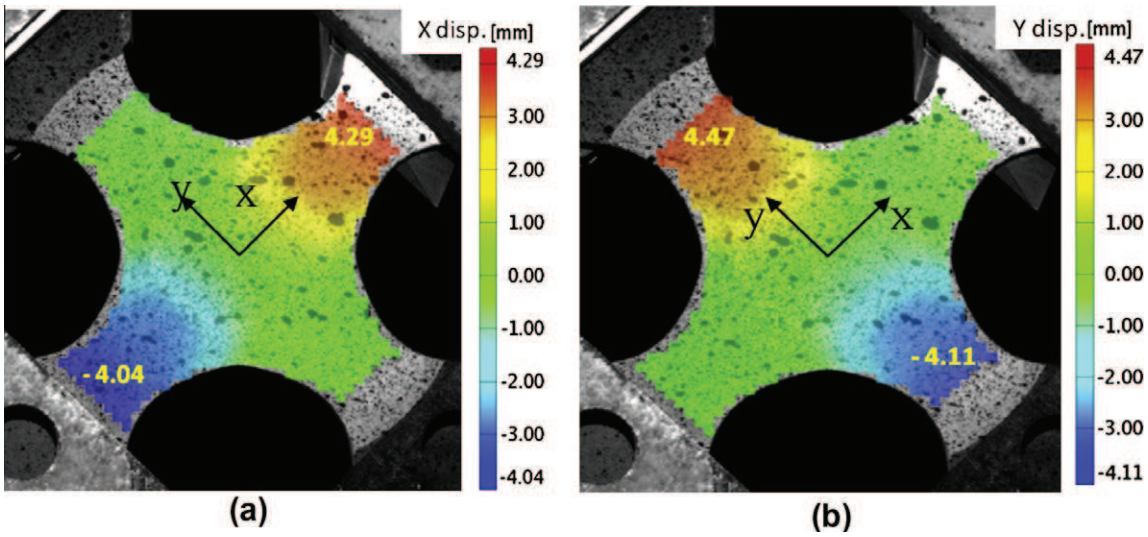

Fig. 5. Typical results obtained by the SIC method (a) displacement in x load direction, and (b) displacement in y load direction.

4. Numerical simulation

4.1. Ductile damage model

In some applications, such as metal forming, safety–critical applications (aircraft, nuclear, aerospace and so on,) the ability of the designer to predict mechanical failure become an important factor. In 1977, Gurson [20], proposed a micro-structural criterion of ductile materials. This yield condition concerns a modification of the isotropic von Mises yield criterion. This model is one of the important contributions for material degradation analysis and describes the mechanism of internal damaging in the form of void growth in porous metals. In the original version of Gurson mode the matrix material was assumed to be incompressible, rigid-perfectly plastic, and the resulting macroscopic model is compressible rigid-plastic with hardening and softening associated. This model was extended in 1984 by Tvergaard and Needleman [19] who incorporated some additional parameters (q_1, q_2, q_3). The formulation is nowadays known as the GTN model, it describes the nucleation, propagation and coalescence of voids. Recently, the GTN

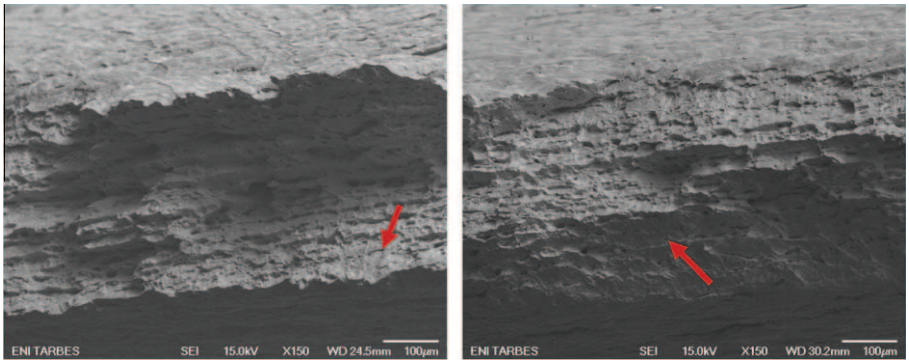

Fig. 6. SEM image showing shear fracture mechanism.

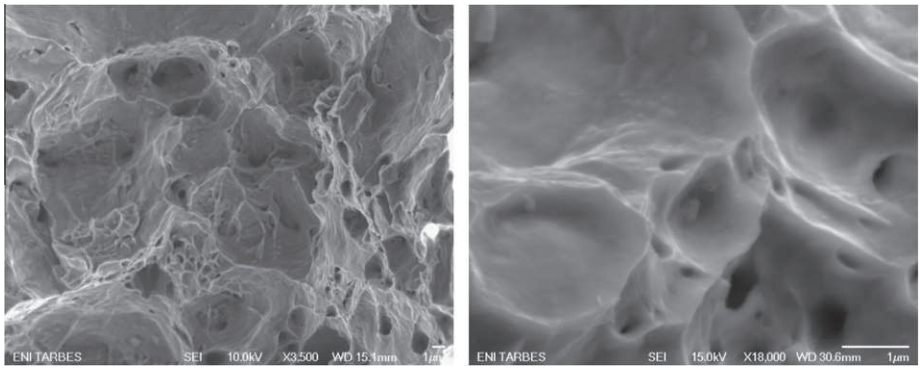

Fig. 7. SEM image showing dimples with second phase particles.

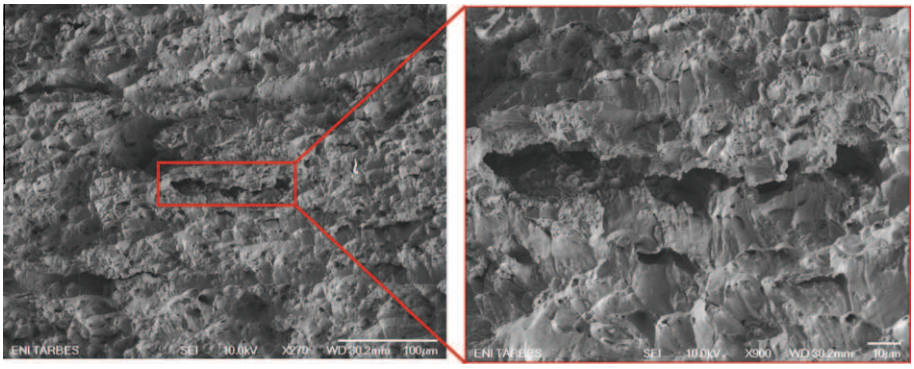

Fig. 8. SEM image showing the coalescence of voids.

model has been investigated by many researchers. Chen and Dong [21], for instance, used GTN model coupled with Hill'48 yield criterion to predict the necking and the failure analysis of an anisotropic sheet metal forming. Furthermore, the GTN model has demonstrated that it is able to predict correctly the failure onset in sheet metal forming part [16,22,23].

Kumar [24] indicate the one drawback of the GTN-model, namely its incapability to model discrete fracture, but it can be ideally combined with discrete crack models. In this context, Vajragupta et al. [25] utilized GTN damage model coupled with a unit cell model to determinate the damage curve of the ferrite.

The yield function describing the plastic constitutive model is represented as flows:

$$\varphi(\sigma,\sigma_m,f)=\frac{\overline{\sigma^2}}{\sigma_y^2}+2f^*q_1\cosh\left(\frac{3}{2}q_2\frac{\sigma_m}{\sigma_y}\right)-(1+q_3(f^*)^2)=0 \qquad (1)$$

where q_1, q_2 and q_3 are a fitting parameters used to a calibrate to the model prediction of periodic arrays of spherical and cylindrical voids, with $q_3=(q_1)^2$, σ_m hydrostatic stress, σ_y yield stress of matrix material, $\overline{\sigma}$: von Mises equivalent stress, f is the void volume fraction which is equal to $1-\frac{V_M}{V}$, f^* represent the modified void volume fraction which is given as follows:

$$f^*=\begin{cases} f & \text{if} \quad f\leqslant f_c \\ f_c+\frac{f_u^*-f_c}{f_f-f_c}(f-f_c) & \text{if} \quad f>f_c \end{cases} \qquad (2)$$

where f_u^* represent the ultimate value of f^* which is defined as the stress carrying capacity vanishes, f_F represent the void volume fraction corresponding to failure, and f_c is the critical volume fraction where rapid coalescence occurs.

The instantaneous rate of growth of the void fraction depends both on nucleation of new voids and growth of pre-existing voids and it is given by:

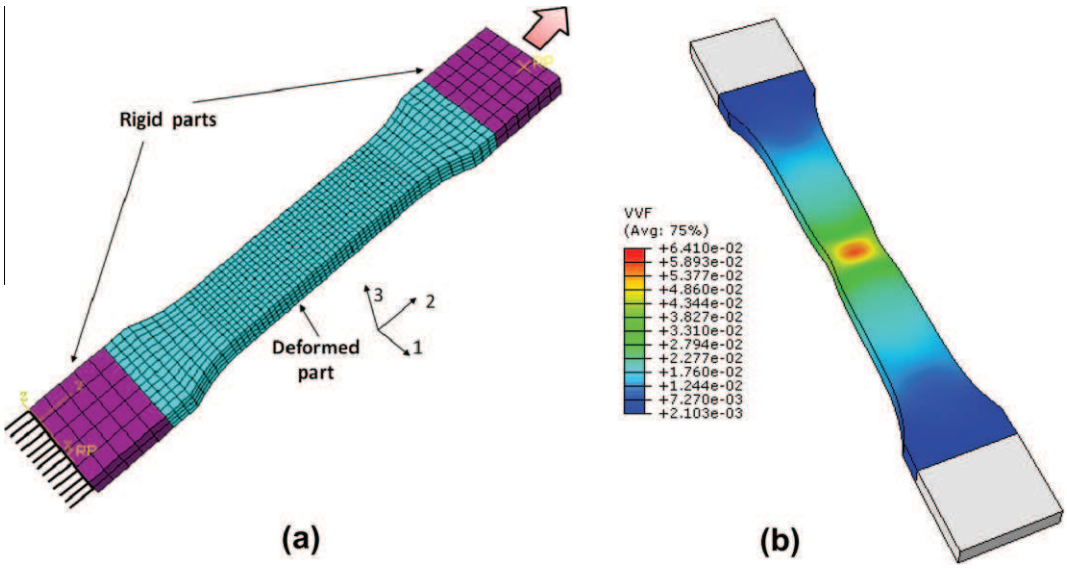

Fig. 9. (a) FE model of uniaxial tensile test, and (b) damage, volume fraction.

$$df = \underbrace{(1-f)\cdot(d\varepsilon_{kk}^{p})}_{growth} + \underbrace{a d\bar{\varepsilon}^{p}}_{nucleation} \tag{3}$$

where ε_{kk}^{p} is the plastic hydrostatic strain and a defined as follows:

$$a = \frac{f_N}{S_N \cdot \sqrt{2\pi}} \cdot \exp\left[-\frac{1}{2}\cdot\left(\frac{\bar{\varepsilon}_p - \varepsilon_N}{S_N}\right)^2\right] \tag{4}$$

where S_n the standard deviation, ε_n the mean effective plastic strain of nucleation and f_n the nucleation micro-void volume fraction.

For GTN application in finite elements simulation we need these parameters:

- The elasticity parameters E and v.
- The power hardening parameters K and n The parameters q_1 and q_2 governing the voids' growth, which are determined from numerical micromechanics analysis. In most cases good results for metals are obtained with $q_1 \approx 1.5$ and $q_2 \approx 1$ were recommended by Tvergaard and Needleman [22].
- The initial void volume fraction and the nucleation parameters f_N, ε_N, and s_N can be estimated, $\varepsilon_N = 0.3$ and $S_N = 0.22$ and $f_N = 0.04$ are reasonable values for metals.
- It is the same for the coalescence parameters f_F and f_c where estimations from numerical simulations and experiments on metals are $f_F = 0.12$ and $f_c = 0.08$.

4.2. Uniaxial tensile test simulation

The objective of the numerical simulations of tensile test is to predict the localization of deformation and in the subsequent step to identify different parameters of the necking criterion. In the following, the uniaxial tensile test is simulated numerically using a 3D FE model under commercial software abaqus, the same geometry is used in experimental tensile test modeled by deformable elements, the specimen is meshed by more than 2688 3D hexahedral elements (C8D8R). Two rigid bodies connect with the specimen to represent the gripping heads of the machine (Fig. 9a). This model takes into account the ductile damage of sheet metal by using GTN model, Fig. 9b shows the volume fraction map in the tensile test specimen.

4.3. Biaxial tensile test simulation

The design and preparation of the cruciform biaxial tensile specimen to solve the problems of the non-uniform stress distribution in the central region and small deformation is not so straightforward. For this reason, several FE models are developed, by varying the geometry of the cruciform specimen. Fig. 10a shows the finite elements model of the cruciform selected geometry. The dimensions of this model are already presented in previous

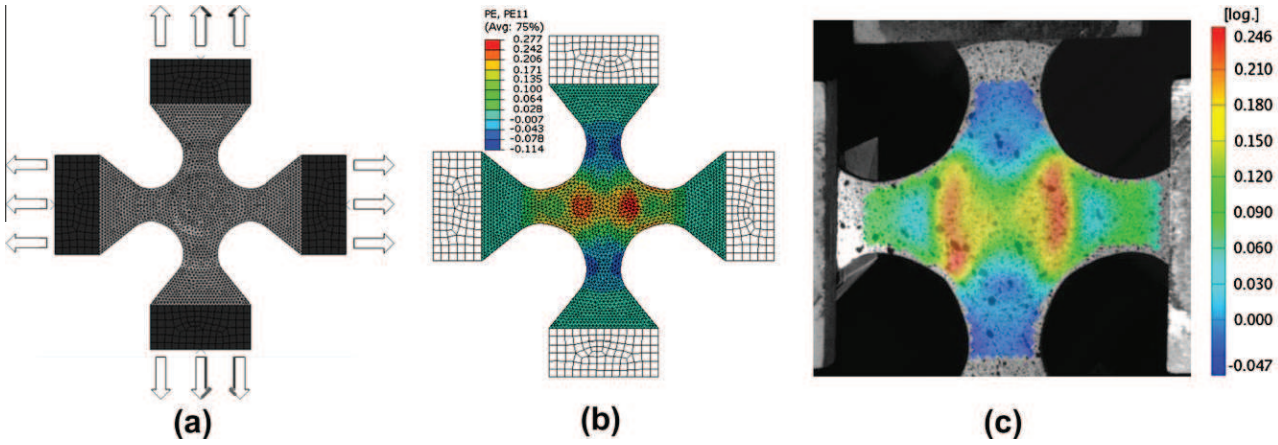

Fig. 10. (a) Numerical model of biaxial test, (b) numerical results of strain distribution in cruciform specimen and (c) experimental strain map obtained by SIC method.

section Fig. 3. The model of the cruciform specimen was meshed by more than 28,000 linear tetrahedral elements (C3D4). Also, the GTN model is used to predict the damage phenomenon on the cruciform sample during biaxial loading. Fig. 10b and c shows numerical and experimental strain distribution in the horizontal direction (x direction) respectively. A good correlation between these two results is observed.

5. Necking and localization of deformation

In low ductile materials, tensile failure occurs by the formation of an inclined groove where the plasticity is localized. Necking is an important limitation on material formability in sheet metal forming [26]. It appears that there are two basic geometrically nonlinear causes of the necking instability: (i) a decrease of the cross-section area of the specimen, causing a stress increase for the same load value, and (ii) the formation of micro voids leading to damage evolution and drastically decrease of the material properties in the metal [27,16]. Often, damage and fracture models have been used to study the governing factors of localization in the sheet metal forming process. The pioneering work elaborated by Considère in 1885, based on experimental observations, proposed that the onset of necking of a tensile round bar to be the attainment of the maximum pulling force [28,29]. For the simple tension Considerer's equation is written:

$$\frac{d\sigma_{11}}{d\varepsilon_{11}} = \sigma_{11} \tag{5}$$

In the 50's Swift [30] extended this diffuse necking theory for biaxially stretched sheets. And Hill [31] developed the first theory for local necking. He assumed the existing of a narrow band in the sheet where in the strains along the band direction vanishes. Onset of localized neck indicates that critical limit strains have been exceeded and thus heralds imminent failure [32]. Fig. 11a and b illustrates experimental and numerical results of the shape of cross section in the central zone of specimen respectively. With concordance of the results presented by Ghajar et al. [33], the rectangular section, in plastic deformation, necking occurs and causes the sides of minimum section to bend as shown in Fig. 11a. A qualitative comparison between the areas at fracture and the corresponding to numerical modeling testifies the robustness of numerical model. As demonstrated in this modeling, the failure is expected to initiate in the center of the minimum section in the specimen [34,35]. Fig. 12a and b shows, respectively, the numerical and experimental results of the diffuse and local necking in tensile test, also an evaluation of strain distribution throughout a section parallel of the load axis. Two phases of necking are visible in the successive digital images of the sample surface during the tensile test on the SIC results computed by the Aramis software and in the numerical results. The necking evolution starts by a symmetric diminution of the width of the specimen. This one is called the diffuse necking. If the diffuse necking is progressing, the severe thickness reduction that mainly takes place at the center of the sample causes a sudden initiation of a crack that immediately propagates in an unstable form along only one shear band. This latter is called the local necking. Generally, in the sheet metal forming the diffuse necking is

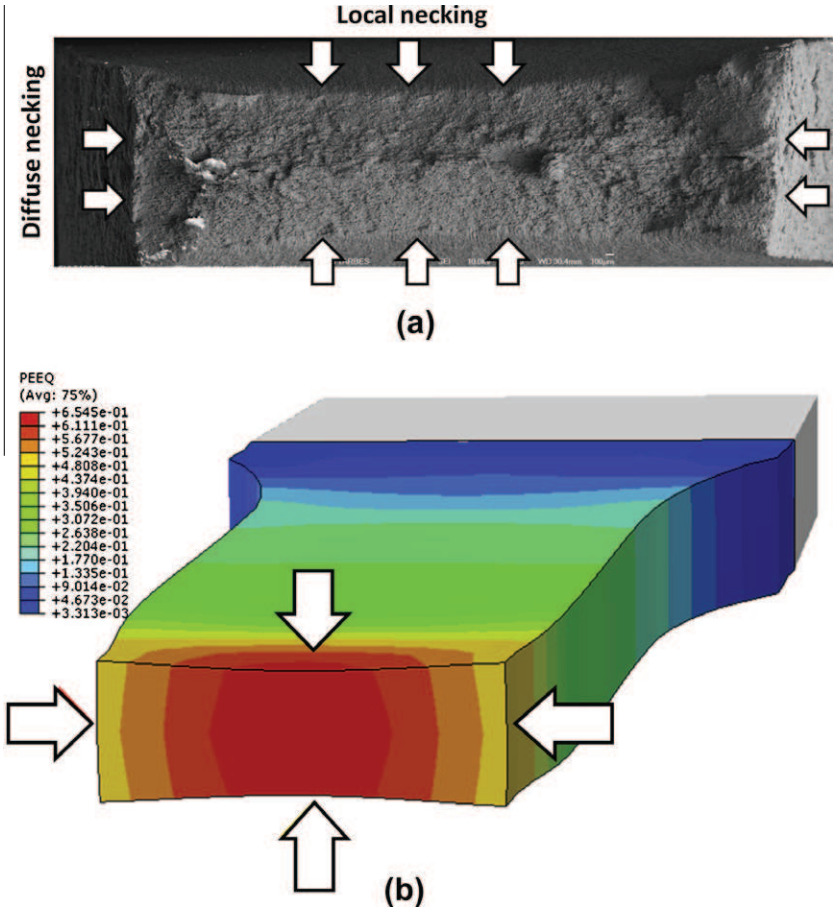

Fig. 11. (a) Experimental area at fracture showing the ductile rupture initiation at the center of the section and (b) numerical prediction of the shape of central zone after tensile (necking).

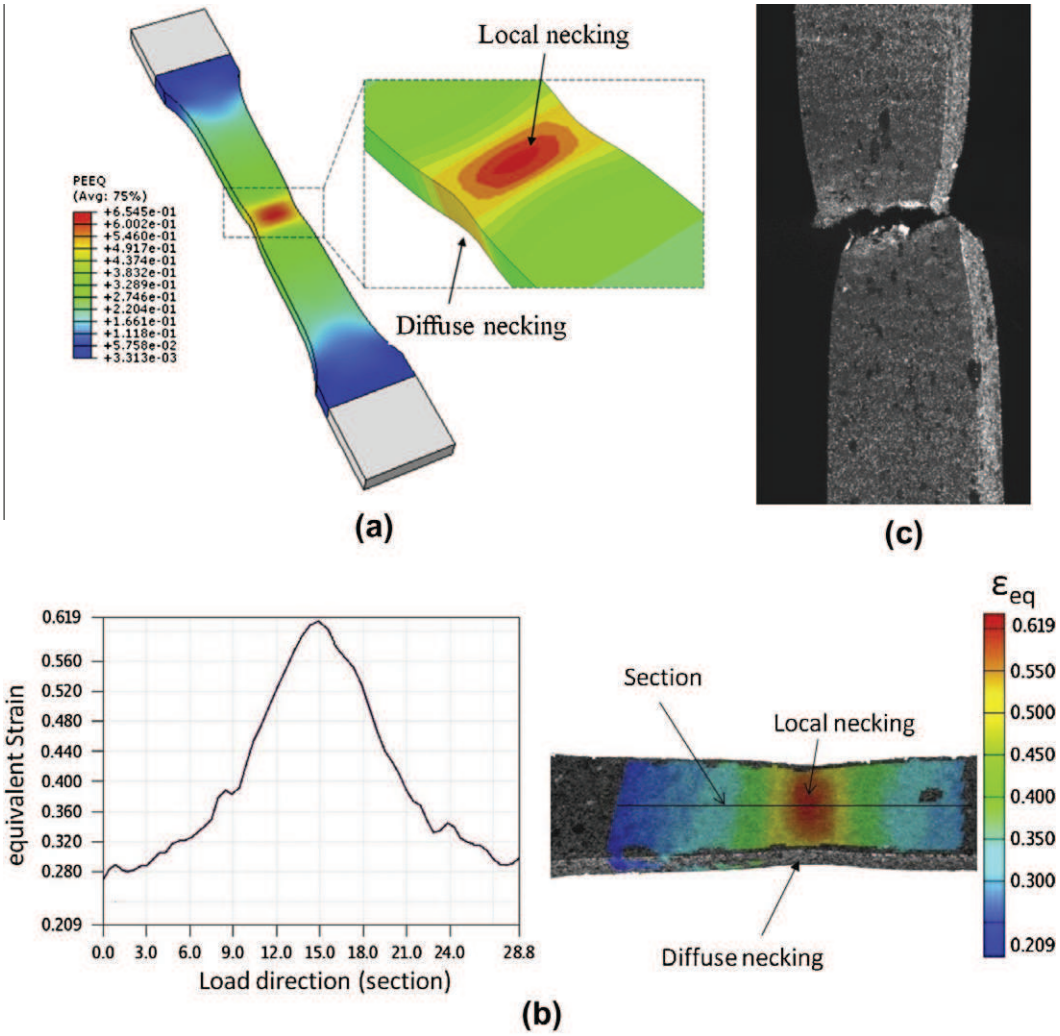

Fig. 12. Deformation localization: diffuse necking and local necking (a) numerical result (b) experimental result obtained by SIC, and (c) specimen after fracture.

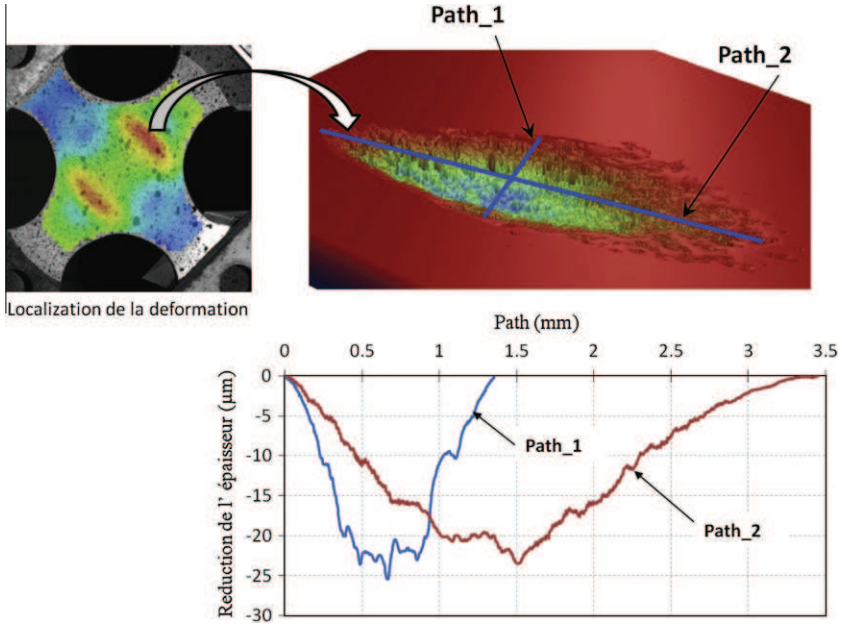

Fig. 13. Experimental evaluation of localization of deformation obtained by digitalization of localization using optical profile projector.

considered as the first trace of failure [32]. The localization of deformation analysis in the sheet metal forming process has attracted a great deal of the numerical and the experimental effort to understand the phenomenon. In most of the sheet metal forming process will have the presence of biaxial stress. Notably, this can be observed in the bulge test, the stretch test and the tube hydroforming. Fig. 12c shows that the final failure path is along the transverse direction, which is in coherence with the results published by Hu et al. [36]. This author claims that if width/thickness ratios such as $w/t \leqslant 6$ two conjugate localized necking bands form during deformation after the onset of necking and the evolution of deformation at the intersection of the two bands developed the failure propagation along the transverse direction. Fig. 13 shows the result of digitalization using optical profile projector. The localization of deformation in the central zone of the cruciform specimen and the thickness reduction principally was measured in four local zones. The local reduction of thickness can attain 25 μm in elliptical shape.

6. Conclusion

This investigation of localization and necking attracted great interests to engineers, as a prior indication of ultimate structural failure. In metal-forming processes, these phenomena can be considered as principal reason for poor product quality. In the current study, experimental and numerical observations are carried out to investigate the failure process in mild steel. Several experimental tests are conducted using mild steel. Stereo Image Correlation is used to obtain full-field displacements in uniaxial and biaxial tests. The deformation in the gauge area is localized by means of two slowly evolving diagonally oriented shear bands that intersect the corners of the gauge area. No homogeneity of deformation on the specimen surface is observed. From the fractography, it is observed that the failure process of the material is due to damage initiation, growth, propagation and crack nucleation within the material. Numerically, the plastic damage of mild steel are studied using the finite element model based on GTN ductile damage constitutive equations. Moreover, in depth analysis of necking phenomenon is developed based on the numerical and experimental results.

References

[1] Baldi A, Medda A, Bertolino F. Comparing two different approaches to the identification of the plastic parameters of metals in post-necking regime. In: Proceedings of the SEM annual conference, Indianapolis, Indiana, USA, June 7–10, 2010.
[2] Koc P, Stok B. Computer-aided identification of the yield curve of a sheet metal after onset of necking. Comput Mater Sci 2004;31:155–68.
[3] Joun M, Choi I, Eom J, Lee M. Finite element analysis of tensile testing with emphasis on necking. Comput Mater Sci 2007;41:63–9.
[4] Hu X, Wilkinson DS, Jain M, Mishra RK. A parametric finite element study and an analytical model of particle distributions on post-necking deformation and failure mode in AA5754 aluminum alloy sheets. Int J Fract 2010;164:167–83.
[5] Becker R. An analysis of shear localization during bending of a polycrystalline sheet. J Appl Mech-Trans ASME 1992;59:491–6.
[6] Dao M, Lie M. A micromechanics study on strain-localization-induced fracture initiation in bending using crystal plasticity models. Philos Mag A 2001;81:1997–2020.
[7] Hu X, Jain M, Wilkinson DS, Mishra RK. Microstructure-based finite element analysis of strain localization behavior in AA5754 aluminum sheet. Acta Mater 2008;56:3187–201.
[8] Wu PD, Lloyd DJ, Jain M, Neale KW, Huang Y. Effects of spatial grain orientation distribution and initial surface topography on sheet metal necking. Int J Plast 2007;23:1084–104.
[9] Needleman A. Material rate dependence and mesh sensitivity in localization problems. Comput Methods Appl Mech Eng 1988;67:69–85.
[10] Ghosh AK. Strain localization in the diffuse neck in sheet metal. Metall Mater Trans B 1974;5(7):1607–16.
[11] Garbowski T, Maier G, Novati G. On calibration of orthotropic elastic–plastic constitutive models for paper foils by biaxial tests and inverse analyzes. Struct Multidiscip Optim 2012;46(1):111–28.
[12] William Sharpe N. Springer handbook of experimental solid mechanics. Springer; 2008.
[13] Dumoulin S, Tabourot L, Chappuis C, Vacher P, Arrieux R. Determination of the equivalent stress–equivalent strain relationship of a copper sample under tensile loading. J Mater Process Technol 2003;133:79–83.
[14] Hannon A, Tiernan P. A review of planar biaxial tensile test systems for sheet metal. J Mater Process Technol 2008;198:1–13.
[15] Narayanasamya R, Sathiya Narayananb C. Forming limit diagram for Indian interstitial free steels. Mater Des 2006;27:882–99.
[16] Abbassi F, Belhadj T, Mistou S, Zghal A. Parameter identification of a mechanical ductile damage using Artificial Neural Networks in sheet metal forming. Mater Des Volume 2013;45:605–15.
[17] Narayanasamya R, Sathiya Narayananb C. Evaluation of limiting strains and strain distribution for interstitial free steel sheets while forming under different strain conditions. Mater Des 2007;28:1555–76.
[18] Bonora N, Gentile D, Pirondi A, Newaz G. Ductile damage evolution under triaxial state of stress: theory and experiments. Int J Plast 2005;21:981–1007.
[19] Tvergaard V, Needleman A. Analysis of the cup–cone fracture in a round tensile bar. Acta Metall 1984;32:157–69.
[20] Gurson AL. Continuum theory of ductile rupture by void nucleation and growth and flow rules for porous ductile media. J Eng Mater Technol 1977;99(1):2–15.
[21] Chen Z, Dong X. The GTN damage model based on Hill'48 anisotropic yield criterion and its application in sheet metal forming. Comput Mater Sci 2009;44:1013–21.
[22] Abbasi M, Bagheri B, Ketabchi M, Haghshenas DF. Application of response surface methodology to drive GTN model parameters and determine the FLD of tailor welded blank. Comput Mater Sci 2012;53:368–76.
[23] Ramazani A, Abbasi M, Prahl U, Bleck W. Failure analysis of DP600 steel during the cross-die test. Comput Mater Sci 2012;64:101–5.
[24] Kumar V. Modeling ductile fracture using a simplified meshfree method. Comput Mater Sci 2013;67:296–302.
[25] Vajragupta N, Uthaisangsuk V, Schmaling B, Münstermann S, Hartmaier A, Bleck W. A micromechanical damage simulation of dual phase steels using XFEM. Comput Mater Sci 2012;54:271–9.
[26] Viatkina EM, Brekelmans WAM, Geers MGD. A crystal plasticity based estimate for forming limit diagrams from textural inhomogeneities. J Mater Process Technol 2005;168:211–8.
[27] Bazant ZP, Luigi C. Stability of structures: elastic inelastic fracture and damage theories, 2003.
[28] Considère A. Mémoire sur l'emploi du fer et de l'acier dans les constructions. Annales des ponts et chassées 1885;9:574.
[29] Marciniak Z, Duncan JL, Hu SJ. Mechanics of sheet metal forming, second ed., 2002.
[30] Swift W. Plastic instability under plane stress. J Mech Phys Solids 1952;1:1–18.
[31] Hill R. On discontinuous plastic states, with special reference to localized necking in thin sheets. J Mech Phys Solids 1952;1:19–30.
[32] Rao KP, Sing WM. On the prediction of the effect of process parameters upon forming limit strains in sheet metals. Int J Mech Sci 2000;42:451–72.
[33] Ghajara R, Mironeb G, Keshavarza A. Ductile failure of X100 pipeline steel – experiments and fractography. Mater Des 2013;43:513–25.
[34] Bonora N, Ruggiero A, Gentile D, De Meo S. Practical applicability and limitations of the elastic modulus degradation technique for damage measurements in ductile metals. Strain 2011;47:241–54.
[35] Oh C-S, Kim N-H, Kim Y-J, Baek J-H, Kim Y-P, Kim W-S. A finite element ductile failure simulation method using stress-modified fracture strain model. Eng Fract Mech 2011;78:124–37.
[36] Hu XH, Wilkinson DS, Jain M, Wu PD, Mishr RK. The impact of particle distributions and grain-level inhomogeneities on post-necking deformation and fracture in AA5754 sheet alloys during uniaxial tension. Mater Sci Eng A 2011;528:2002–16.